

Optical reflectivity and magnetoelectric effects on resonant plasmon modes in composite metal-multiferroic systems

H. Vivas C.

*Departamento de Física, Universidad Nacional de Colombia, Sede Manizales, A.A. 127, Col.**

C. Vargas-Hernández

Grupo de las Propiedades Ópticas de los Materiales (POM)

Departamento de Física, Universidad Nacional de Colombia, Sede Manizales, A.A. 127, Col.

(Dated: March 22, 2013)

The rôle of the magnetoelectric effect upon optical reflectivity is studied by adapting an electrodynamic-based model for a system composed by a 2D metallic film in contact with an extended multiferroic material exhibiting weak ferromagnetism. The well-known *Nakayama's* boundary condition is reformulated by taking into account the magnetoelectric coupling as well as an externally applied magnetic field \mathbf{B} in arbitrary direction. It is found that the relative reflectance shows strong fluctuations for in-plane \mathbf{B} -fields and might be controllable under its azimuthal rotation in the THz regime, in particular, close to the antiferromagnetic resonance frequency associated to the multiferroic slab.

Keywords: Multiferroics, Magnetoelectric effect, Surface Plasmon, Reflectance.

DOI: PACS numbers: 73.20.-e, 75.82.+t, 78.20.Bh, 78.66.Bz

I. INTRODUCTION

Magnetoelectric (ME) effects in multiferroic (MF) or ferromagnetic (metallic) films have brought remarkable interest since promising technological applications in spintronics and ultrafast electric field control on magnetic data storage are seen as imminent^{1,2}. Characterization of the relative strength for the ME coupling can be obtained by implementing terahertz spectroscopy in rare earth manganites of the type RMnO_3 ($\text{R}=\text{Tb}$, Gd , Dy , Eu:Y)^{3,4,5,6} demonstrating that the generated electromagnons (mixed spin-waves and photon states) represent, among others, the signature of the ME effect for an approximate range of frequencies between 10 cm^{-1} to 40 cm^{-1} at temperatures where antiferromagnetic resonance modes (AFMR) coexist, or more recently, the key mechanism for controllable magnetochromism in $\text{Ba}_2\text{Mg}_2\text{Fe}_{12}\text{O}_{22}$ hexaferrites⁷. The primary origin for the ME coupling is commonly associated to the Dzyaloshinskii-Moriya relativistic exchange-interaction^{8,9} which is appropriate for the description for asymmetric spin wave dispersion on double layer Fe-films¹⁰ as well as for those materials where weak ferromagnetism emerges, namely the Ilmenite FeTiO_3 , TbMnO_3 , $\text{Eu}_{1-x}\text{Y}_x\text{MnO}_3$ ($0 < x \lesssim 0.3$ at $T < 40\text{ K}$)¹¹ or the widely studied pyroelectric ferromagnet BaMnF_4 ¹². Weak ferromagnetism on this compound is generated by canting effects between antiferromagnetic sub-lattices, leading into a spontaneous polarization \mathbf{P} perpendicular to the resulting magnetization \mathbf{M} ¹³. Considerations in the symmetry change of the static polarization and magnetization fields have brought interesting unconventional optical phenomena labeled as non-reciprocal dichroism associated to the sign reversal of $\mathbf{P} \times \mathbf{M}$, recently reported in the perovskite $\text{Eu}_{0.55}\text{Y}_{0.45}\text{MnO}_3$, with magnetoelectric activity for photon energies around 0.8 meV

(sub THz regime) in the cycloidal phase at 4 K ¹⁴. Intense activity in the last decade has also been dedicated to achieve possible optical and photonic band gap control via Surface Plasmon (SP) propagation in periodic arrays¹⁵, since modern lithographic techniques allows to design functional objects with almost any geometrical pattern at sub-wavelength scale¹⁶. Plasmon localization and its coupling with incident light depend on the dielectric properties of the metal in conjunction of its surrounding environment, enlightening an alternative route for engineering highly efficient SP photonic devices via externally applied fields, rare earth doping or electron charge transference from the modified metal¹⁷. In this communication we study an electrodynamic-based model for estimating the optical response generated by the contact between a material exhibiting weak ferromagnetism in contact with a 2D metallic film. It is found that a specific strength of the ME interaction might couple with localized charge-sheet modes for electron carrier densities close to 10^{16} cm^{-2} and incident frequencies around 18 cm^{-1} , leading into a change in the reflectance from the metallic film. Applied magnetic field effects on relative reflective are also discussed in section III.

II. MODEL

Localized charge-sheet modes in a 2D conducting medium in the framework of Drude approximation is obtained from the Nakayama result^{18,19,20}:

$$\frac{\varepsilon_1}{\kappa_1} + \frac{\varepsilon_2}{\kappa_2} = -\frac{ic^2\sigma}{\omega} = \frac{\Omega_S c}{\omega^2}, \quad (1)$$

where $\kappa_j = (q_Y^2 - \varepsilon_j \omega^2 / c^2)^{1/2}$, ($j = 1, 2$) corresponds to the quasiwavevector in Y -direction, Ω_S is defined as $\nu e^2 / \varepsilon_0 m c$ and ν denotes the electron density concentration in a two dimensional space. The term ε_j

represents the relative dielectric function value for j -th medium, with $\varepsilon_1 = 1$ for vacuum. In the range of wavelengths behind the far infrared radiation (< 1 mm), the dielectric function approaches to the well recognized Lyddane-Sachs-Teller (LST) relationship: $\varepsilon_2 \approx (1 + \chi_\infty)(\omega_L/\omega_T)^2$, where χ_∞ corresponds to the dielectric permittivity of the medium $j = 2$ and $\omega_{L,(T)}$ represents the longitudinal (transverse)-optical phonon frequency. For numerical purposes, we have set $(\omega_L/\omega_T)^2 \approx 1.07$, which coincides with the relationship for the b -axis normal phonon modes in BaMnF₄. The permittivity χ_∞ is a functional depending on mechanical strain deformations and polarization field depletion in the proximities between the multiferroic slab and metal film²¹, and is taken as constant for zero applied (electric) field and fixed temperature. Formula (1) is derived by solving the complete set of Maxwell equations with normal (TM wave) incidence for $Z > 0$, and boundary conditions on the plane $Z = 0$ with the *ansatz* for propagating fields $\mathbf{E}, \mathbf{H} \sim e^{-\kappa_2 Z} e^{-i(q_Y Y - \omega t)}$ in the region $Z < 0$. Magnetoelectric effects are taken into consideration throughout the transverse susceptibility χ^{me} and the electric displacement vector \mathbf{D} is written into the constitutive equation like $\mathbf{D} = \varepsilon_2 \mathbf{E} + 4\pi\chi^{me} \mathbf{H}$. After inserting the additional term $4\pi\chi^{me} \mathbf{H}$, the expression (1) shall be modified under $\kappa_2 \rightarrow \kappa_2 + 4\pi i\omega\chi^{me}/c$. In the plane $Z = 0$, and in agreement with the geometrical configuration showed in Figure (1), the non-zero surface current density component is defined as $J_Y = \sigma E_Y$, where σ corresponds to the σ_{YY} -element of the generalized conductivity tensor²², and E_Y is the electrical field propagating on Z direction. The generic

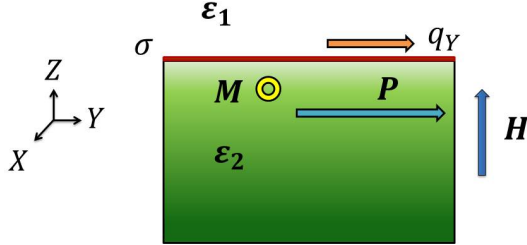


FIG. 1: Conducting Charge-Sheet in contact with a multiferroic surface. The polarization vector \mathbf{P} and the wavevector of coupled excitations q_Y are also depicted in the diagram. *Weak ferromagnetic* magnetization vector \mathbf{M} is produced by interacting antiferromagnetic sublattices with relative canting angle θ_C .

expression for the transverse susceptibility χ^{me} is obtained from first principles^{23, 24} and it can be summarized as: $4\pi i\omega\chi^{me}/c = 2\pi icg\omega \left[(\omega_p^2 - \omega^2)^{-1} - (\omega_m^2 - \omega^2)^{-1} \right]$, where $g \equiv g(\theta_C, \mathbf{M}, \mathbf{P}, \omega_m, \omega_p)$ is a coupling param-

eter which is an involved function of the canting angle between two adjacent (antiferromagnetic) sublattices, the spontaneous magnetization \mathbf{M} and the polarization vector \mathbf{P} , as well as the parameters $\omega_{m(p)}$. g is conveniently given in units of mm^{-2} all throughout this paper²⁵, in concordance with the spectral weight intrinsically associated to the fitting procedure for the transmittance spectra via Lorentzian model in various multiferroic species, namely RMn₂O₅ (R:Y,Tb), TbMnO₃ or LuMnO₃²⁶, and its dependence with the externally applied magnetic field has been neglected for small canting angles (See for instance Eqns. (38) and (47) in ref. (13)). Two main poles are clearly identified for χ^{me} : the optical antiferromagnetic resonance mode (AFMR) ω_m and the soft-phonon along \mathbf{M} with resonance frequency ω_p , with $\omega_p > \omega_m$. Classical plasmon excitations in low 2D carrier electron density are experimentally detected and theoretically estimated for wavevectors $q \lesssim 1.4 \text{ cm}^{-1}$ and frequencies $\omega \lesssim 0.5 \text{ meV}$ ^{27, 28, 29}, therefore the condition $q_Y^2 \gg \varepsilon_j \omega^2 / c^2$ remains valid in the range of interest, and the dispersion relationship for the coupled magnetoelectric plasma mode is obtained by solving the modified equation (1):

$$q_Y^\pm = \frac{1}{2} \left[Q \pm \sqrt{Q^2 - \gamma_2 \left(\frac{\omega}{2\pi c} \right)^2 \left(Q - \gamma_1 \left(\frac{\omega}{2\pi c} \right)^2 \right)} \right], \quad (2)$$

with $Q = 4\pi i\omega\chi^{me}/c + \gamma_1 (\omega/2\pi c)^2$, $\gamma_1 = 4\pi^2 c(\varepsilon_1 + \varepsilon_2)/\Omega_S$ and $\gamma_2 = 16\pi^2 c\varepsilon_1/\Omega_S$. For $\chi^{me} = 0$, i.e., no magnetoelectric effects taken under consideration, we reproduce the expression for the localized plasmon mode¹⁸:

$$\omega = \sqrt{\frac{4\pi^2 c^2 q_Y}{\gamma_1}}, \quad (3)$$

where (+) sign in equation (2) has been selected. Complex index of refraction $\tilde{n}(\omega)$ is directly estimated from the wavenumber³⁰ $q_Y : \tilde{n}(\omega) = cq_Y/\omega$. The lowest-order reflectance coefficient $R(\omega)$ for normal incidence is defined as $R(\omega) = |\tilde{n}(\omega) - 1|^2 / |\tilde{n}(\omega) + 1|^2$ and its numerical profile discussed on the next section.

III. RESULTS AND DISCUSSION

Figure (2) exhibits the reflectance response as a function of the 2D electronic carrier concentration ν , for different wavelengths and the magneto-electric coupling parameter g fixed at 0.02. Dotted curve (a) is set as reference for $g = 0$. In this case, reflectivity minima are located at wavelengths $\lambda_c = 2\pi(\varepsilon_1 + \varepsilon_2)c/\Omega_S$, or $\lambda_c^{-1} \propto \nu$, indicating that the critical wavelength for *bare* plasmon excitations is larger as the electronic concentration decreases. The AFMR mode lies in the range THz range, with $\omega_m \sim 0.54 \text{ THz}$, while the transverse phonon frequency is taken as 7.53 THz for the BaMnF₄ compound³¹. Metallic behavior predominates for concentrations higher than 10^{18} cm^{-2} and smaller than 10^{16}

cm^{-2} and selected wavelengths between 0.4 mm and 0.7 mm. Plasmonic resonance effects are important for carrier densities around 10^{17} cm^{-2} , where radiative absorption or antireflective phenomena become strong and the reflectance spectrum is therefore significantly modified by diminishing the percentage of absorbed radiation only when the external frequency approaches the characteristic mode ω_m , and $g \neq 0$. Figure (3) depicts the shift-

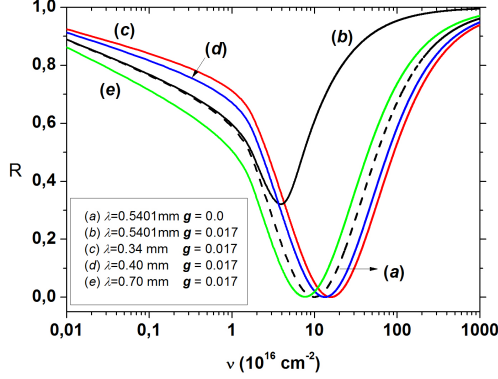


FIG. 2: Zero field reflectance response as a function of electron carrier density ν . Curves (a) and (b) correspond to responses with $g = 0$ and $g \sim 0.02$ respectively, close to the optic antiferromagnetic resonance mode ω_m .

ing of the minimum of reflectance in the (ν, g) plane. The ME effect becomes relevant by decreasing the critical carrier density ν_c as g increases, and it remains unmodified for those frequencies far away from the AFMR characteristic mode as indicated in lines (d) and (e). ν_c shall be understood as the electron carrier concentration which maximizes the antireflective effect for the composite metal/multiferroic system. Applied magnetic field \mathbf{B} enters into the formalism by taking symmetry considerations upon the dependence of the electrical conductivity as a function of \mathbf{B} under the transformation $\sigma \rightarrow \sigma(B)$, with $\sigma(B) = i\Omega_{sc}^{-1}\omega(\omega^2 - \omega_B^2)^{-1}$, and $\omega_B = eB/m$ as the cyclotron frequency. Expression (2) changes as $q_Y^\pm =$

$$\frac{1}{2} \left[Q' \pm \sqrt{Q'^2 - \gamma_2 \frac{(\omega^2 - \omega_B^2)}{(2\pi c)^2} \left(Q' - \gamma_1 \frac{(\omega^2 - \omega_B^2)}{(2\pi c)^2} \right)} \right], \quad (4)$$

with $Q' = Q - \gamma_1 \omega_B^2 / (2\pi c)^2$. The classical localized magnetoplasmon mode (3) is rewritten for $g = 0$ and under B as³²:

$$\omega = \sqrt{\omega_B^2 + \frac{4\pi^2 c^2 q_Y}{\gamma_1}}, \quad (5)$$

in similarity with result (3). In this particular case, the antireflective condition ($\tilde{n} = 1$) depends on the external magnetic field intensity as $\lambda_c^{-1} = \pi/\gamma_1 + \sqrt{(\pi/\gamma_1)^2 + (\omega_B/2\pi c)^2}$, which leads into a quadratic

correlation $\lambda_c^{-1} \propto B^2$ for $\gamma_1 \omega_B / 2\pi^2 c \ll 1$. For an orientation of \mathbf{B} , equation (1) shall be modified on its right side accordingly with $\Omega_{sc}\omega^{-2} \rightarrow \Omega_{sc}(\omega^2 - \omega_B^2)^{-1} F(n_X, n_Y, n_Z)$, where $F(\cdot)$ is a function of the directors $n_{X,Y,Z}$ ³³. Maximum change in the relative reflectivity takes place for $B \parallel X$ -axis (Voigt configuration) and parallel to \mathbf{M} , while no significant (or zero) variation in $\Delta R/R = R(B)/R(0) - 1$ ³⁴ comes out for $B \parallel Y$ -axis, suggesting that an *effective* rotation on the weak magnetization vector \mathbf{M} generates quasi-periodic fluctuations upon the optical activity close to the antiferromagnetic resonance frequency and diminishes coherence in the collective excitations propagating along Y -direction, as shown in figure (4). *In-plane* applied field \mathbf{B} effects on the reflectance as a function of carrier density ν are illustrated in Fig. (5). $R(\mathbf{B})$ tends to augment for \mathbf{B} parallel to X -axis and decreases for \mathbf{B} along $-X$ axis. Curve (b) for null \mathbf{B} overlaps the outcome of R for $B = 1.5$ T, $\phi = \pi/2$ (i.e., parallel to Y axis) and the same g parameter, indicating no substantial variation in the optical reflectance for applied fields in the same direction of the plasmonic wavevector q_Y . Strong fluctuations around the baseline $\Delta R = 0$ in the relative reflectance factor $\Delta R/R$ are mainly observed for wavelengths close to the AFMR frequency $2\pi c/\omega_m$, and their intensities tend to decrease for stronger ME couplings (See figures (6) and (8)). These effect does not appear when the g is set as zero (not shown), suggesting a direct correlation between the *dressed* confined plasmonic excitations at the Drude metal, the intensity of the applied field and its optical response. Dotted line (e) in Fig. (7) is set as reference for B perpendicular to the plane $Z = 0$ for parameters corresponding to curve (b) in Figure (6). Figure (7) shows the reflectivity response for externally applied fields parallel to the $Z = 0$ plane as a function of the incident wavelengths. Iso-reflective lines for $\Delta R/R$ close to $2\pi c/\omega_m$ and the externally applied magnetic field (in Z direction) are shown in Figure (9). Projected lines preserve symmetrical distribution under magnetic field inversion but it changes for wavelengths around $2\pi c/\omega_m$ and $g > 0$, i.e., regardless the applied magnetic field orientation, the relative reflectance flips its sign at $2\pi c/\omega_m$. The reflectance function $R(B)$ reaches values from $0.2R(B=0)$ to $0.8R(B=0)$ for intensities lying in the interval $0.52 < B < 2.3$ T. On the edge of the THz bandwidth, i.e. $\lambda_E \sim 1$ mm, the reflectance factor $R(\lambda_E)$ remains constant (around 0.1) for magnetic field intensities lesser than 3 T and augments exponentially up to ~ 0.4 for $3 < B < 8$ T and $g = 0.02$. In the limit of the microwave band ($\lambda_M \sim 10$ mm), $R(\lambda_M)$ changes from 0.8 to 0.96 for $0 < B < 1$ T with no significant influence of ME coupling on the metallic behavior.

IV. CONCLUDING REMARKS

We have developed a model for studying the magneto-electric interactions on 2D plasmonic modes in the THz range for a metal/multiferroic device. The multiferroic

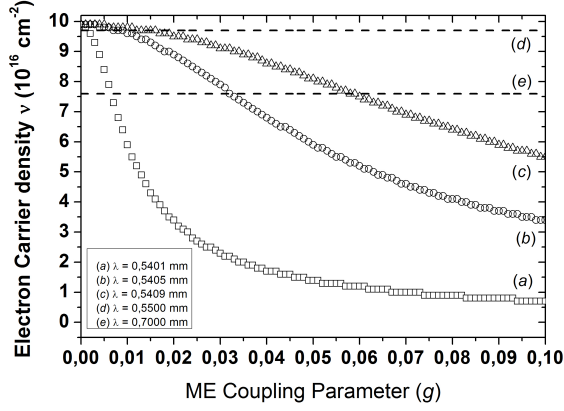


FIG. 3: Critical carrier density ν_c as a function of the ME coupling parameter g for different wavelengths. ν_c is strongly depending on g only for external frequencies close to AFMR mode ω_m .

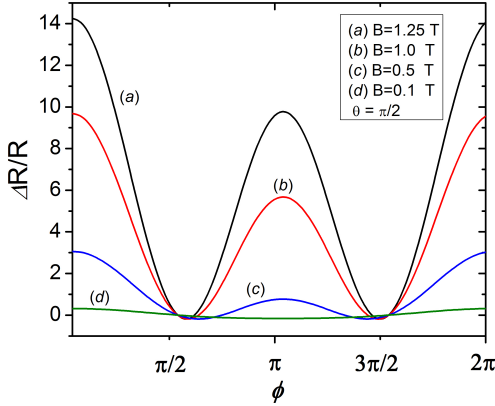


FIG. 4: Relative Reflectance factor for *in-plane* applied magnetic field close to AFMR frequency at $2\pi c/\omega = 0.53$ mm, at $g = 0.02$ as a function of azimuthal angle ϕ .

medium exhibits weak ferromagnetism and the metallic behavior enters into the formalism in the framework of the classical Drude-Lorentz model. Relative reflectance response for normal incidence is numerically calculated for different ME coupling strengths and wavelengths close to the optical antiferromagnetic resonance frequency ω_m . Characteristic soft phonon and AFMR

numerical values were taken for BaMnF_4 , showing that a particular condition for antireflectivity might be adjustable by varying the intensity of the applied field, its orientability or the incident frequency of radiation in a range $\omega > \omega_m$, while the zero field reflectance increases up to 60% for a change in the ME coupling around to $\Delta g = 0.02 \text{ mm}^{-2}$. The quantity $R(B)$ at $B = 1\text{T}$

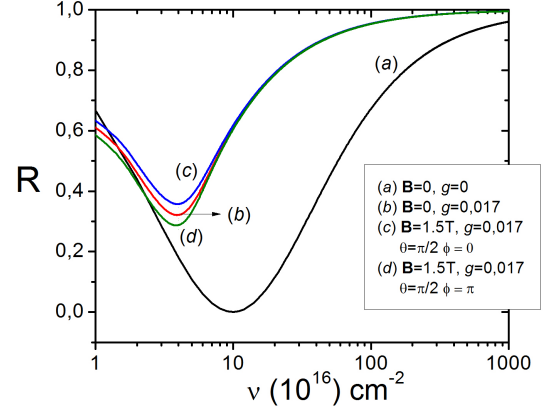


FIG. 5: Reflectance as a function of electron carrier density for *in-plane* applied field \mathbf{B} and $2\pi c/\omega = 0.53$ mm. Line (a) corresponds to uncoupled ($g = 0$) response.

parallel to the X axis reaches values up to $10R(0)$ in contrast with approximately $1.2R(0)$ for the same field intensity but for \mathbf{B} perpendicularly applied to the XY plane, indicating notorious enhancement in the value of the relative reflectance in the former case. Although all numerical simulations were conducted for $\varepsilon_2 = K\varepsilon_1$ (K being a positive number), simultaneous electric field control \mathbf{E}_0 on optical properties for the composite device might also be achieved under the dielectric function dependence for a multiferroic material $\varepsilon_2[\mathbf{P}(\mathbf{E}_0)]$, the polarization $\mathbf{P}(\mathbf{E}_0)$ and temperature, issue that shall be addressed in further investigations.

Acknowledgments

H.V. wants to thank computing accessibility at POM group. C. V-H. acknowledges financial support provided by DIMA, *Dirección de Investigación Sede Manizales*, Universidad Nacional de Colombia. H.V. declares no competing financial interest.

* Electronic address: hvivasc@unal.edu.co

¹ C-G Duan, J. P. Velez, R. F. Sabirianov, Z. Zhu, J. Chu, S. S. Jaswal and E. Y. Tsymlal, Phys. Rev. Lett. **101**, 137201 (2008).

² L. Gerhard, T. K. Yamada, T. Balashov, A. F. Takács, R. J. H. Wesselink, M. Däne, M. Fechner, S. Ostanin, A. Ernst, I. Mertig and W. Wulfhekel, Nature Nanotechnology **5**, 792 (2010). doi:10.1038/nnano.2010.214

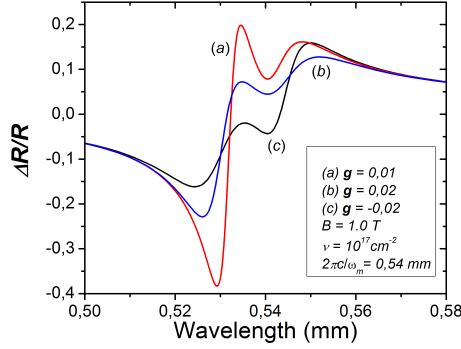


FIG. 6: $\Delta R/R$ for $B = 1$ T and different ME coupling parameters g with $\theta = 0$.

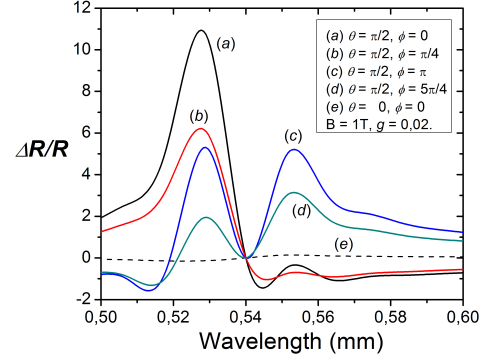


FIG. 7: Change in the relative reflectivity response $\Delta R/R$ for applied magnetic fields parallel to $Z = 0$ plane, $\nu = 10^{17} \text{ cm}^{-2}$.

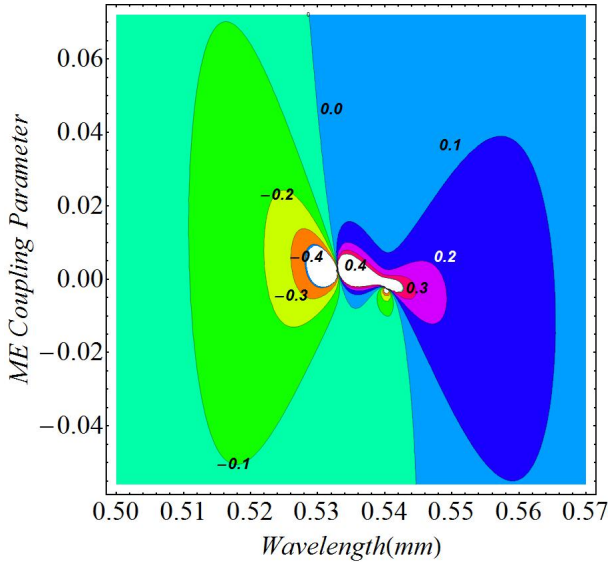


FIG. 8: Contour lines for relative reflectance response in the (λ, g) parametric plane, with $B = 1$ T and $\nu = 10^{17} \text{ cm}^{-2}$.

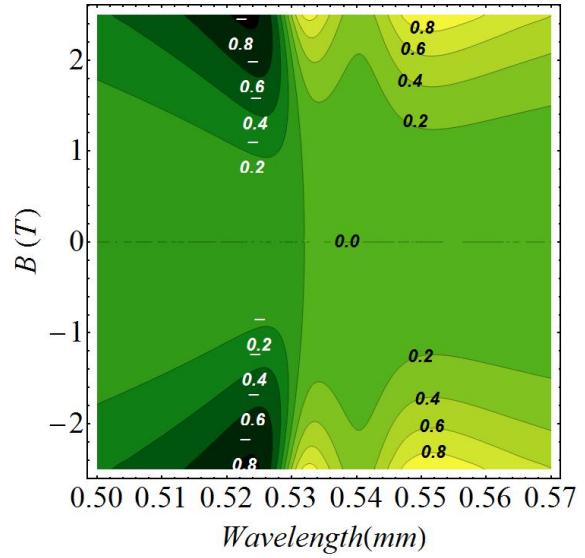


FIG. 9: Isorefective lines of $\Delta R/R$ under applied magnetic fields with $\nu = 10^{17} \text{ cm}^{-2}$, $g = 0.02$ and $2\pi c/\omega_m = 0.54 \text{ mm}$.

- ³ A. Pimenov, A. M. Shuvaev, A. A. Mukhin and A. Loidl, J. Phys.: Condens. Matter **20**, 434209 (2008).
- ⁴ D. Talbayev, S. A. Trugman, A. V. Balatsky, T. Kimura, A. J. Taylor and R. D. Averitt, Physical Review Letters **101**, 097603 (2008).
- ⁵ H. Němec, F. Kadlec, P. Kužel, L. Duvillaret and J.-L. Coutaz, Optics Communications **260**, 175 (2006).
- ⁶ A. Pimenov, A. A. Mukhin, V. Yu Ivanov, V. D. Travkin, A. M. Balbashov and A. Loidl, Nature Physics **2**, 97-100 (2006).
- ⁷ N. Kida and Y. Yokura, Journal of Magnetism and Magnetic Materials **324**, 3512 (2012).
- ⁸ H. Katsura, N. Nagaosa and A. V. Balatsky, Physical Review Letters **95**, 057205 (2005).
- ⁹ H. Katsura, A. V. Balatsky and N. Nagaosa, Physical Review Letters **98**, 027203 (2007).
- ¹⁰ Kh. Zakeri, Y. Zhang, J. Prokop, T.-H. Chuang, N. Sakr, W. X. Tang and J. Kirschner, Physical Review Letters **104**, 137203 (2010).
- ¹¹ A. A. Mukhin, V. Yu Ivanov, V. D. Travkin, A. S. Prokhorov, A. A. Volkov, A. V. Pimenov, A. M. Shuvaev and A. Loidl, Phys.-Usp **52**, 851 (2009). DOI: 10.3367/UFNe.0179.200908j.0904
- ¹² J. F. Scott, Rep. Prog. Phys. **42**, 1055 (1979).
- ¹³ V. Gunawan and R. L. Stamp, J. Phys.: Condensed Matter **23**, 105901 (2011).
- ¹⁴ Y. Takahashi, R. Shimano, Y. Kaneko, H. Murukawa and Y. Tokura, Nature Physics **8**, 121 (2012), doi:10.1038/nphys2161
- ¹⁵ W. L. Barnes, A. Dereux and T. W. Ebbensen, Nature **424**, 824 (2003).
- ¹⁶ S. Li, M. Jadidi, T. E. Murphy and G. Kumar, Optical Express **21** No. 6, 7041 (2013).
- ¹⁷ H. J. Freund, Surface Science **601**, 1438 (2007).
- ¹⁸ M. Nakayama J. Phys. Soc. Jpn. **36**, 393 (1974).
- ¹⁹ M. Cottam and D. R. Tilley, *Introduction to Surface*

- and *Superlattice Excitations*, Cambridge University Press (1989).
- ²⁰ J. M. Pitarke, V. M. Silkin, E. V. Chulkov and P. M. Echenique, Rep. Prog. Phys. **70**, 1-87 (2007).
 - ²¹ S. Zhong, S. Alpay, V. Nagarajan, J. Mater. Res. **21** (6) (2006) 1600.
 - ²² J. Sólyom, *Fundamentals of the Physics of Solids*, Vol. II, Springer-Verlag (2009).
 - ²³ D. R. Tilley and J. F. Scott, Physical Review B **25**, 3251 (1982).
 - ²⁴ K. L. Livesey and R. L. Stamps, Physical Review B **81**, 094405 (2010).
 - ²⁵ J.-P. Rivera, Eur. Phys. J. B. **71**, 299 (2009).
 - ²⁶ A. B. Sushkov, R. Valdés Aguilar, S. Park, S-W. Cheong and H. D. Drew, Physical Review Letters **98**, 027202 (2007).
 - ²⁷ E. H. Hwang and S. Das Sarma, Physical Review B **64**, 165409 (2001).
 - ²⁸ I. A. Nechaev, V. M. Silkin and E. V. Chulkov, Journal of Experimental and Theoretical Physics **112**, Issue 1, pp 134-139 (2011).
 - ²⁹ F. Kanjouri, A. H. Esmailian and M. Molayem, Eur. Phys. J. B **79**, 429 (2011).
 - ³⁰ G. R. Fowles, *Introduction to Modern Optics*, Second Edition, Dover (1989); J. B. Marion and M. A. Heald, *Classical Electromagnetic Radiation*, Second Edition, Chapter 6, Academic Press (1980).
 - ³¹ J. Barnaś, Journal of Magnetism and Magnetic Materials **62**, 381 (1986).
 - ³² M. A. Eriksson, A. Pinczuk, B. S. Dennis, C. F. Hirjibehedin, S. H. Simon, L. N. Pfeiffer, K.W. West, Physica E **6**, 165 (2000).
 - ³³ $F(n_X, n_Y, n_Z) = H_1 + H_2$, with $H_1 = 1 - \omega_B^2 n_Y^2 / \omega^2$, $H_2 = -q_Y (\omega_B n_X / \omega - i \omega_B^2 n_Y n_Z / \omega^2) (q_Y + 4\pi i \omega \chi^{me} / c)^{-1}$ and $n_X = \sin \theta \cos \phi$, $n_Y = \sin \theta \sin \phi$ and $n_Z = \cos \theta$.
 - ³⁴ J. D. E. McIntyre and D. E. Aspnes, Surface Science **24**, 417 (1970).